Check for updates

Co$_3$O$_4$–Ag photocatalysts for the efficient degradation of methyl orange†

Hongmei Chen, [a] Chenyang Xue, [*a] Danfeng Cui, [a] Maoxing Liu, [b] Yi Chen, [a] Yuankai Li[a] and Wendong Zhang[*a]

In this paper, a series of Co$_3$O$_4$–Ag photocatalysts with different Ag loadings were synthesized by facile hydrothermal and *in situ* photoreduction methods and fully characterized by XRD, SEM, TEM, FTIR spectroscopy, XPS, UV-vis and PL techniques. The catalysts were used for the degradation of methyl orange (MO). Compared with the pure Co$_3$O$_4$ catalyst, the Co$_3$O$_4$–Ag catalysts showed better activity; among these, the Co$_3$O$_4$–Ag-0.3 catalyst demonstrated the most efficient activity with 96.4% degradation efficiency after 30 h UV light irradiation and high degradation efficiency of 99.1% after 6 h visible light irradiation. According to the corresponding dynamics study under UV light irradiation, the photocatalytic efficiency of Co$_3$O$_4$–Ag-0.3 was 2.72 times higher than that of Co$_3$O$_4$ under identical reaction conditions. The excellent photocatalytic activity of Co$_3$O$_4$–Ag can be attributed to the synergistic effect of strong absorption under UV and visible light, reduced photoelectron and hole recombination rate, and decreased band gap due to Ag doping. Additionally, a possible reaction mechanism over the Co$_3$O$_4$–Ag photocatalysts was proposed and explained.

1. Introduction

Water pollution, which affects human health and the healthy development of the whole ecosystem, is becoming more and more serious with the rapid development of industries.[1] To date, many types of treatments for water pollution have been developed by researchers,[2,3] but the main drawbacks such as severe reaction conditions or complicated processes significantly limit their practical applications. In contrast, since previous research has reported that TiO$_2$ can be used for water splitting and organic pollutant degradation,[4,5] the use of semiconductors as photocatalysts has attracted increasing attention due to their perfect utilization of the clean and renewable solar energy.[6–9] However, TiO$_2$ can only absorb ultraviolet light due to its wide band gap ($\sim$3.2 eV).[10–14] Hence, various new types of semiconductors have been developed as photocatalysts to solve this problem.[15–26] Among these, Co$_3$O$_4$ is a potential material for many applications because of its excellent electronic and magnetic properties.[6,27,28] For example, it can be used as a material for supercapacitors due to its high theoretical capacitance ($\sim$3560 F g^{-1}).[29–31] Additionally, it can be applied in various photocatalytic reactions because it is non-toxic,

environmentally friendly and cost-efficient.[32] Nevertheless, the Co$_3$O$_4$ nanoscale materials still suffer from some difficulties in real industrial applications. The photocatalytic efficiencies of simple Co$_3$O$_4$ nanomaterials are often low due to the fast recombination rate of photoelectrons and holes. Thus, it is really a challenge for researchers to design and explore new kinds of promising Co$_3$O$_4$ photocatalysts with higher efficiency. To date, various methods have been used to improve the catalytic activity of Co$_3$O$_4$ photocatalysts. For example, constructing p–n heterojunctions such as Co$_3$O$_4$/ZnO,[33] Co$_3$O$_4$/Bi$_2$WO$_6$,[34] Co$_3$O$_4$/TiO$_2$,[35] and Bi$_2$O$_3$/Co$_3$O$_4$ (ref. 36) is effective. Besides, doping noble metals into simple metal oxides can improve the photocatalytic activity.[37] Among the noble metals, elemental Ag is widely used due to its lower cost. Its role in improving the catalytic activity mainly involves two aspects. First, Ag doping can separate the photogenerated carriers efficiently because of the formation of a Schottky barrier.[38,39] Second, it can improve the response to visible light.[40,41] The positive role of Ag as a cocatalyst has been reported in several catalytic systems, such as TiO$_2$,[41,42] SnO$_2$,[43] and Cu$_2$O.[44] However, to date, doping elemental Ag in the Co$_3$O$_4$ system for MO degradation has rarely been reported.

Most of the previous studies have focused on Co$_3$O$_4$ materials and satisfactory progress has been made for pollutant degradation. However, there are still some problems for practical applications. First, the recovery and reuse of granular materials are difficult. Then, the product separation process after the reaction is complex and requires considerable energy. Finally, the mass loss of the materials is serious. On the

^{a}*Science and Technology on Electronic Test and Measurement Laboratory, North University of China, Taiyuan, Shanxi 030051, China. E-mail: xuechenyang@nuc.edu.cn; wdzhang@nuc.edu.cn*

^{b}*Department of Mathematics, Qingdao University of Science and Technology, Qingdao, 266061, China*

contrary, materials coated on substrates have potential as they are easy to use and separate. However, the photocatalytic efficiencies of simple Co_3O_4 catalysts are still low. Hence, in this paper, a series of highly active Co_3O_4–Ag catalysts on Ni foam substrates were prepared for the degradation of MO. High activity with 96.4% degradation efficiency was achieved after 30 h UV light irradiation, and high degradation efficiency of 99.1% could be obtained after 6 h visible light irradiation over the Co_3O_4–Ag-0.3 photocatalysts. The impacts of the Ag additive on the structure, morphologies, and chemical properties of the photocatalysts were investigated thoroughly.

2. Experimental

2.1. Preparation of the photocatalysts

All chemicals were of analytical reagent (AR) grade and used as received without any further treatment.

Synthesis of Co_3O_4. The Ni foam substrates (2.5 cm × 2.5 cm) were washed with acetone, muriatic acid, ethanol and deionized water in turn with ultrasonication for 10 min. Typically, 1.75 g $Co(NO_3)_2 \cdot 6H_2O$ and 18 mL deionized water were mixed and stirred for 5 min; 12 mL ammonia solution was then dropped into the above solution for another 30 min under magnetic stirring. Finally, the above mixture and the Ni substrate were transferred into a 50 mL Teflon-lined stainless-steel autoclave and kept at 120 °C for 10 h. Then, the Ni substrate-covered precursor was washed with deionized water and dried. Finally, the obtained particles were calcined at 250 °C for 2 h to acquire the Co_3O_4 materials.

Preparation of Co_3O_4–Ag. Co_3O_4–Ag was synthesized by the *in situ* photoreduction of $AgNO_3$. In detail, the above Co_3O_4 materials were added into 50 mL $AgNO_3$ aqueous solutions of different concentrations and irradiated under UV light for 3 h. After washing with deionized water and drying at 60 °C for 5 h, the final products were labeled as Co_3O_4–Ag-x; x stands for the weight percentage of Ag in the products, for example, Co_3O_4–Ag-0.3 represents that the mass percentage of Ag is 0.3%.

2.2. Characterizations

XRD patterns were obtained from 15° to 85° using a D2 Phaser desktop/max-RAX-ray diffractometer (Bruker, Germany) with Cu Kα radiation at 30 kV and 10 mA. FTIR spectra were measured over a NEXUS Thermo Nicolet IR-spectrometer. XPS was performed on an ESCALAB 250Xi spectrometer. SEM and HRTEM were performed on FEI Inspect F50 and FEI Inspect F30. Ultraviolet-visible (UV-vis) absorption spectra were collected on a DaoJin UV3600 spectrophotometer (Agilent Technologies, USA). The photoluminescence (PL) test was performed on a Raman microscope (Renishaw inVia).

2.3. Photocatalytic activity evaluation

The catalytic activities of all the photocatalysts were evaluated for MO degradation under UV light or visible light ($\lambda > 400$ nm) and the concentration of the MO solutions for all the experiments was 6 mg L^{-1}. The absorbance of the MO solutions was tested using a UNIC UV-2800A spectrophotometer at 465 nm.

First, the Co_3O_4 and Co_3O_4–Ag photocatalysts were placed into the MO solutions (50 mL) for 30 min without irradiation and then, the degradation reaction was performed with ultraviolet light irradiation. During the course of the reaction, certain solutions were taken out and analyzed. For the trapping experiments of the active species for the photocatalytic degradation of MO under UV light, benzoquinone (BQ), isopropanol (IPA) and ethylenediaminetetraacetic acid (EDTA) were used as scavengers and the concentration was 0.001 mol L^{-1}. The absorbances of the MO solutions were recorded immediately after irradiating for 18 h. According to the following formula, the degradation efficiency (D) can be estimated: $D = [(C_0 - C_t)/C_0] \times 100\%$. Here, C_0 is the original absorbance and C_t is the absorbance after a certain sampling time of the MO solution.

3. Results and discussion

3.1. Characterization of the photocatalysts

Fig. 1 displays the XRD patterns of the $Co(OH)_2$, pure Co_3O_4 and Co_3O_4–Ag-0.3 photocatalysts. The obvious peaks at 2θ of 44.5°, 51.8°, and 76.4° corresponded to the (111), (200), and (220) crystal faces of Ni (JCPDS 04-0850) in all samples. The diffraction peaks at 2θ of 19.1°, 37.9°, 38.7° and 57.9° were assigned to the planes of the $Co(OH)_2$ precursor (JCPDS 30-0443). In addition, the peaks positioned at $2\theta = 19.0°$, 36.9°, 38.5°, 55.7°, 59.4°, and 65.2° were assigned to the planes of Co_3O_4 (JCPDS 04-0850) for pure Co_3O_4 and Co_3O_4–Ag-0.3. However, no peaks of
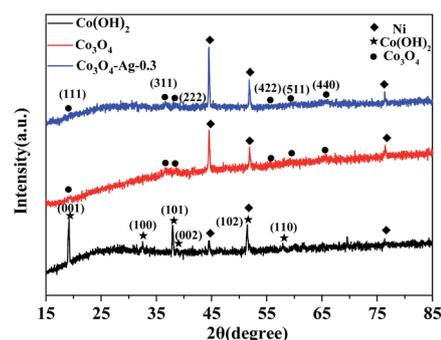

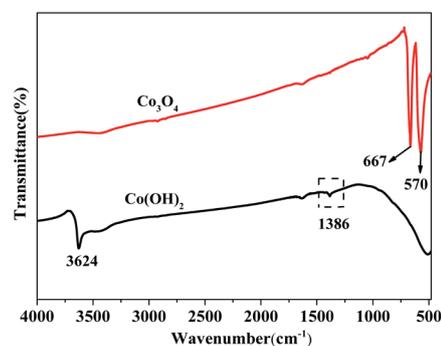**Fig. 1** XRD patterns of $Co(OH)_2$, pure Co_3O_4 and Co_3O_4–Ag-0.3.

Fig. 2 Fourier transform infrared spectra of $Co(OH)_2$ and pure Co_3O_4.

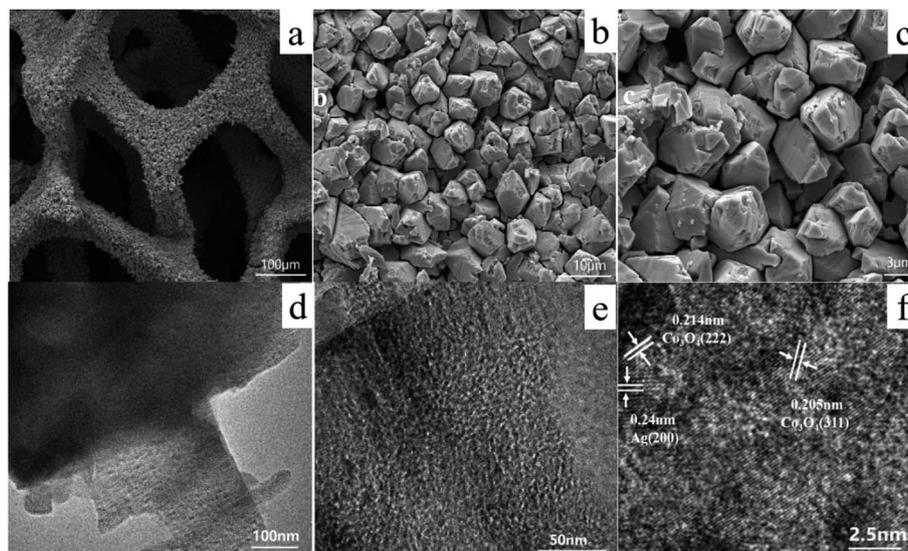**Fig. 3** SEM (a–c) and TEM images (d–f) of Co_3O_4–Ag-0.3.

Ag species were observed because of its low mass in the Co_3O_4–Ag-0.3 sample.

Fourier transform infrared spectroscopy (FTIR) was performed to analyse the surface properties of the catalysts. As depicted in Fig. 2, in the spectrum of $Co(OH)_2$, the band at 1386 cm^{-1} belongs to the bending vibration of the surface adsorbed water, and the peak centered at 3642 cm^{-1} is relevant to the characteristic O–H stretching vibration.[45] Besides, with regard to Co_3O_4, the absorption peaks at 667 and 570 cm^{-1} belong to the fingerprint stretching vibrations of the Co–O bonds, which can evidently signify the formation of Co_3O_4.[46] These results verify the successful synthesis of the $Co(OH)_2$ precursor and Co_3O_4, which is consistent with the XRD data.

Fig. 3 shows the representative SEM and TEM images of Co_3O_4–Ag-0.3. As seen in Fig. 3(a–c), Co_3O_4–Ag-0.3 displays well-developed and defined three-dimensional (3D) "budded flower" morphology. The synthesized Co_3O_4–Ag-0.3 crystals were evenly distributed on the Ni foam substrate and the diameter of the "budded flowers" was about 5.7 μm. Moreover, Fig. 3(d and e) show the images of the nanoparticles of the Co_3O_4–Ag-0.3 catalyst obtained *via* TEM. As illustrated in Fig. 3(f), the lattice spacings of 0.214 and 0.205 nm correspond to the (222) and (311) planes of the Co_3O_4 crystals. Additionally, the lattice spacing of 0.24 nm was assigned to the (200) crystal facet of Ag crystals.[47]
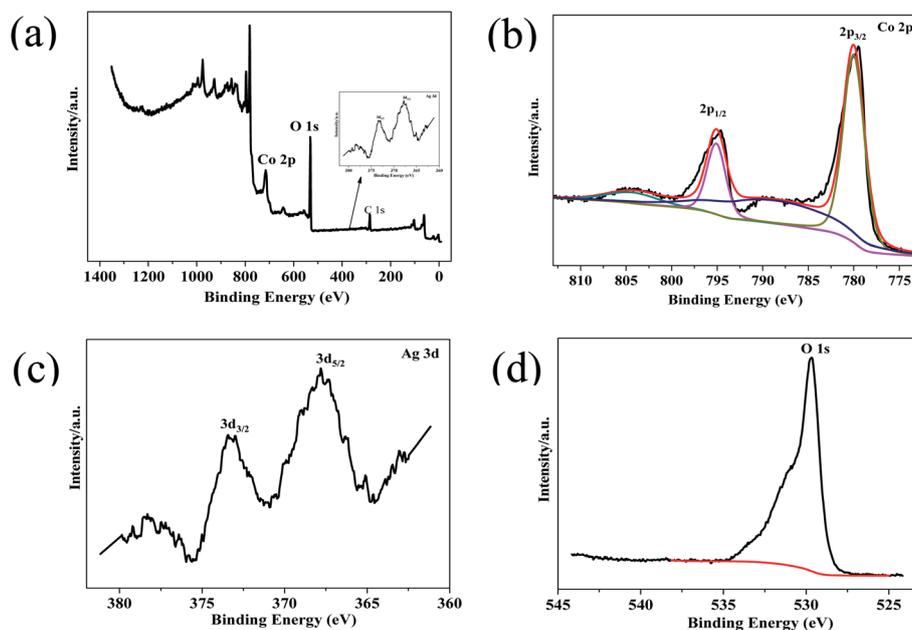

Fig. 4 XPS survey spectrum of Co_3O_4–Ag-0.3 (a), and high-resolution spectra for (b) Co 2p, (c) Ag 3d, and (d) O 1s.

XPS of Co_3O_4–Ag-0.3 was carried out to explore the surface composition and chemical state of the photocatalyst. Fig. 4(a) reveals the presence of Ni, Co, Ag and O in the photocatalyst. The Co 2p spectrum in Fig. 4(b) shows two strong peaks at around 794.86 eV and 779.86 eV. The former peak is attributed to Co $2p_{1/2}$, while the latter belongs to Co $2p_{3/2}$.[48,49] The presence of Co_3O_4 can be further verified by the O 1s XPS peak at 529.66 eV in Fig. 4(d).[50] Fig. 4(c) presents Ag 3d peaks at 373.26 eV and 367.81 eV and they are assigned to Ag $3d_{3/2}$ and Ag $3d_{5/2}$, respectively,[47] indicating the successful deposition of Ag on the Co_3O_4 photocatalyst. Hence the successful formation of Co_3O_4–Ag-0.3 can be inferred, which is in line with the XRD and TEM results.

Additionally, the optical properties of the Co_3O_4 and Co_3O_4–Ag-0.3 photocatalysts were evaluated by UV-vis spectroscopy (Fig. 5). The Co_3O_4 and Co_3O_4–Ag-0.3 photocatalysts exhibited strong absorption under UV and visible light in the ranges of 200–450 and 500–750 nm, respectively.[51,52] The former band belonged to O^{2-}–Co^{2+} and the latter was attributed to the O^{2-}–Co^{3+} charge transfer.[53] As presented in Fig. 6, E_gs are 1.50 eV and 2.04 eV for Co_3O_4, while they are 1.42 eV and 1.95 eV for the Co_3O_4–Ag-0.3 photocatalyst according to the absorption intensities, which are consistent with previous reports.[54,55] The change in E_gs for Co_3O_4 and Co_3O_4–Ag-0.3 may be attributed to the synergy of two aspects. One is the quantum confinement effect in nanomaterials[56] and the other is the dielectric confinement effect, which is similar to that observed for
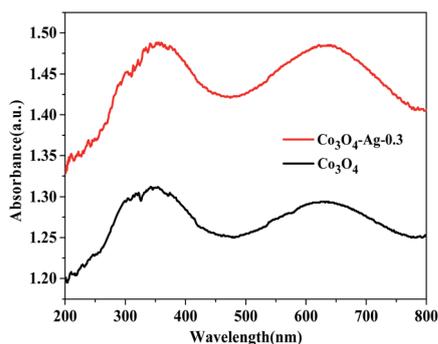

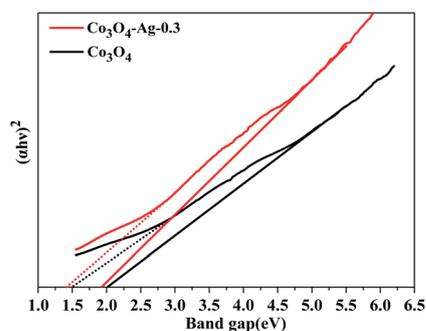**Fig. 5** UV-vis absorption spectra of Co_3O_4 and Co_3O_4–Ag-0.3.

Fig. 6 Plots of $(\alpha h\nu)^2$ *versus* photon energy of Co_3O_4 and Co_3O_4–Ag-0.3.
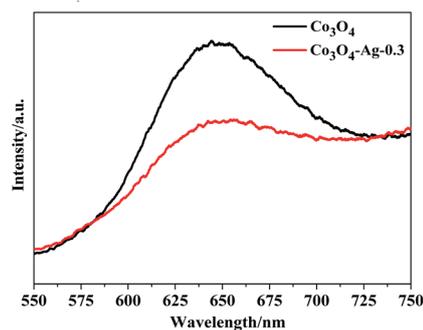
Fig. 7 PL spectra of Co_3O_4 and Co_3O_4–Ag-0.3.

Cu_2O@Ag.[44] From Fig. 5 and 6, it can be revealed that both the UV and visible light absorptions of the composite samples are strengthened, while E_gs become narrower with the addition of Ag compared to that of the pure Co_3O_4 catalyst; this is because Ag doping can restrain the recombination of electrons and holes to endow Co_3O_4–Ag-0.3 with stronger light-harvesting ability to improve the catalytic activity.

The PL spectra of Co_3O_4 and Co_3O_4–Ag-0.3 were obtained at room temperature. Fig. 7 indicates that the excitation wavelength of the PL spectra for the pure Co_3O_4 and Co_3O_4–Ag-0.3 photocatalysts is about 647 nm. However, the Co_3O_4–Ag-0.3 composite photocatalyst showed a weaker emission intensity compared with the pure Co_3O_4 photocatalyst, indicating that the recombination of the photogenerated charge carriers could be inhibited more efficiently over Co_3O_4–Ag-0.3 than over pure Co_3O_4 because of the formation of a Schottky barrier. It is well known that electrons can easily transfer from one material with a lower work function to the other with a higher work function.[57] Thus, the migration of holes from Co_3O_4 to Ag particles was accelerated by the Schottky barrier because of the different work functions of Ag (4.26 eV)[58] and Co_3O_4 (6.2 eV),[59] which could inhibit the photogenerated charge carrier recombination and improve the photocatalytic activity.

3.2. Catalytic performance of the photocatalysts

Fig. 8(a and b) present the relative concentrations of MO solutions at different irradiation times and Fig. S1† shows the corresponding UV-vis spectra of MO over the Co_3O_4–Ag photocatalysts with different Ag loadings. It could be seen that the degradation efficiency for MO was only 6.4% without any photocatalyst. However, MO degraded greatly in the presence of photocatalysts as the irradiation time increased. The degradation efficiency of pure Co_3O_4 for MO was 71.2% after 30 h irradiation. In order to understand the role of different Ag loadings precisely, a series of photocatalysts including Co_3O_4–Ag-0.05, Co_3O_4–Ag-0.15, Co_3O_4–Ag-0.45, and Co_3O_4–Ag-0.6 were synthesized and their degradation efficiency was tested. The degradation activity increased from 89.5% to 96.4% on increasing the loading of Ag from 0.05% to 0.3% after 30 h irradiation. Nevertheless, the degradation efficiency decreased from 96.4% to 79.7% on further increasing the loading of Ag from 0.3% to 0.6%, respectively. Consequently, the
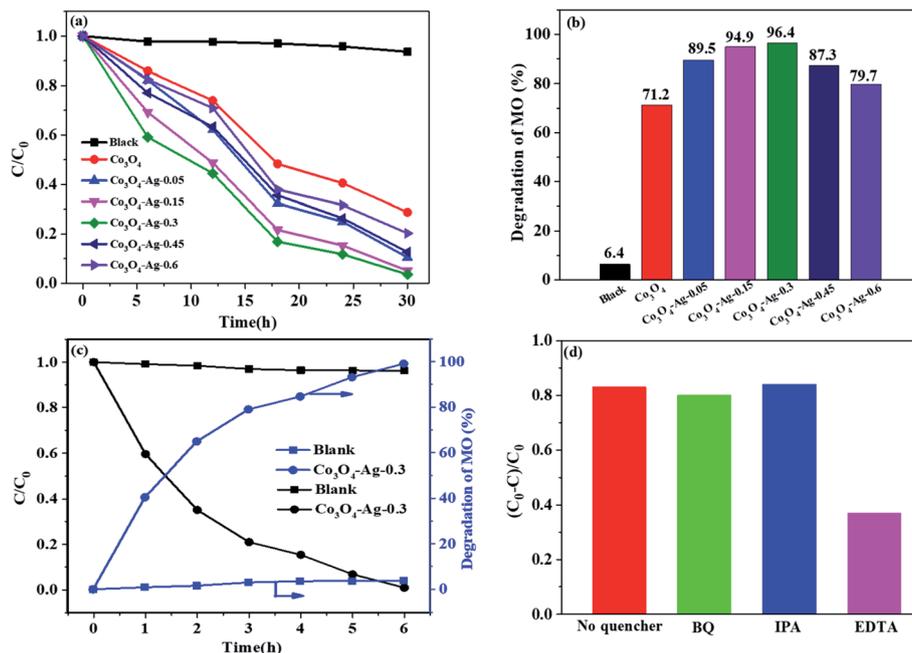
Fig. 8 Degradation rate (a) and degradation efficiency of MO in 30 h (b) over the series of catalysts under UV light. Photocatalytic degradation of MO with or without Co_3O_4–Ag-0.3 under visible light (c). Trapping experiments of the active species during the photocatalytic degradation of MO with Co_3O_4–Ag-0.3 under UV radiation (d).

photocatalytic activity increased with the loading of Ag compared with the activity of pure Co_3O_4, and Co_3O_4–Ag-0.3 showed the most excellent degradation efficiency (96.4%). Furthermore, the kinetics of MO degradation for all catalysts were investigated according to the experimental results. Fig. S2† shows the linear relationship between $\ln(C_0/C)$ and the irradiation time for all the samples. The slope of the catalysts increased from 0.0401 to 0.1091 as the loading of Ag increased from 0.05% to 0.3%, while the slope decreased from 0.1091 to 0.052 when the Ag doping increased from 0.3% to 0.6%, respectively, indicating that the photocatalytic activity of Co_3O_4–Ag-0.3 was 2.72 times that of pure Co_3O_4 at identical reaction conditions. Additionally, we investigated the photocatalytic degradation of MO over the Co_3O_4–Ag-0.3 catalyst under visible light. As shown in Fig. 8(c), the blank experiment indicates that the concentration of MO only slightly decreases without adding catalysts, implying that the photodegradation can be ignored. The degradation efficiency for MO was 99.1% over the Co_3O_4–Ag-0.3 catalyst after 6 h visible light irradiation, which was greatly higher than the degradation efficiency (40.5%) over the same catalyst under UV light irradiation, indicating the excellent visible light-harvesting activity.

The superior degradation performance of the Co_3O_4–Ag catalysts was related to the introduction of Ag. First, as seen in Fig. 3, the structure of Co_3O_4–Ag is uniform and regular. On the other hand, as revealed in Fig. 5 and 6, the absorption intensities for UV and visible light for the Co_3O_4–Ag catalysts significantly increase, while E_gs become narrower with the addition of Ag compared with that for the pure Co_3O_4 catalyst. Moreover, from the PL spectra in Fig. 7, we can infer that the doping of Ag inhibits the recombination of the photogenerated

charge carriers more efficiently than that for pure Co_3O_4 because of the formation of the Schottky barrier, and this is another reason for the excellent catalytic activity of the Co_3O_4–Ag catalysts.

To explain the possible photocatalytic mechanism, trapping experiments of the active species during the photocatalytic degradation of MO over the Co_3O_4–Ag-0.3 catalysts with or without scavengers were performed under UV light. As shown in Fig. 8(d), three scavengers (BQ, IPA, and EDTA) have been adopted. An 83.5% MO degradation efficiency could be obtained over the pure Co_3O_4–Ag-0.3 catalyst. It is well known that BQ and IPA are suitable scavengers of superoxide radicals ($\cdot O_2^-$) and hydroxyl radicals ($\cdot OH$), respectively.[60,61] When BQ and IPA were introduced, the experimental results were almost unchanged, indicating that the superoxide radicals ($\cdot O_2^-$) and hydroxyl radicals ($\cdot OH$) were not the main active species for MO degradation. However, the degradation efficiency decreased greatly to 36.8% in the presence of EDTA, which is the scavenger of holes. Hence, the photogenerated holes (h^+) were concluded to be the main active species for the photocatalytic degradation of MO.

Based on all the above-mentioned results and the trapping experiments of the active species during the photocatalytic degradation of MO, a reaction mechanism was proposed. When Ag was introduced into the Co_3O_4 catalyst, a Schottky junction structure was successfully formed (Fig. 9(a)), which could promote the migration of photo-generated holes from Co_3O_4 to the Ag metal, leaving electrons in the CB of Co_3O_4 because the work function of Co_3O_4 (W_s) was higher than that of the Ag element (W_m),[58,59] as shown in Fig. 9(b). Therefore, the doping of Ag in Co_3O_4 can decrease the recombination rate of the
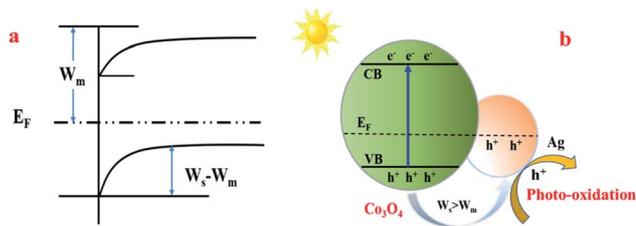
Fig. 9 The proposed reaction mechanism of MO degradation over the Co_3O_4–Ag photocatalysts. W_s: the work function of Co_3O_4; W_m: the work function of Ag; E_F: the balanced Fermi level.

electron–hole pairs and promote the charge separation simultaneously to generate more free holes, which are the main active species for MO degradation, so as to increase the photocatalytic activity effectively.

4. Conclusions

In conclusion, the doping of Ag into Co_3O_4 played a critical role in improving the MO degradation efficiency for the Co_3O_4–Ag photocatalysts using Ni foams as substrates because of the synergistic effect of the strengthened response to UV and visible light, narrower energy gap, and weaker PL intensity. Efficient activity with 96.4% MO degradation efficiency after 30 h UV light irradiation was achieved over the Co_3O_4–Ag-0.3 catalyst, and the photocatalytic activity of Co_3O_4–Ag-0.3 was 2.72 times that of pure Co_3O_4. Meanwhile, an excellent MO degradation efficiency of 99.1% over the Co_3O_4–Ag-0.3 catalyst was obtained after 6 h visible light irradiation. Additionally, a possible photocatalytic reaction mechanism was proposed based on the experimental results. Hence, the Co_3O_4–Ag catalyst covered on the Ni foam is a promising photocatalytic material for pollutant degradation.

Conflicts of interest

There are no conflicts to declare.

Acknowledgements

References

1 Y. Chen, J. Peng, H. Xiao, H. Peng, L. Bu, Z. Pan, Y. He, F. Chen, X. Wang and S. Li, *Appl. Surf. Sci.*, 2017, **420**, 773–781.

2 J. Gómez-Pastora, S. Dominguez, E. Bringas, M. J. Rivero, I. Ortiz and D. D. Dionysiou, *Chem. Eng. J.*, 2017, **310**, 407–427.

3 M. Chong, B. Jin, C. W. K. Chow and C. Saint, *Water Res.*, 2010, **44**, 2997–3027.

4 A. Fujishima and K. Honda, *Nature*, 1972, **238**, 37–38.

5 S. N. Frank and A. J. Bard, *J. Am. Chem. Soc.*, 1997, **99**, 303–304.

6 C. Han, L. Ge, C. Chen, Y. Li, X. Xiao, Y. Zhang and L. Guo, *Appl. Catal., B*, 2014, **147**, 546–553.

7 F. Jing, R. Liang, J. Xiong, R. Chen, S. Zhang, Y. Li and L. Wu, *Appl. Catal., B*, 2017, **206**, 9–15.

8 Y. Sun, G. Wang and K. Yan, *J. Hazard. Mater.*, 2011, **36**, 15502–15508.

9 P. Adriana, L. Vincent, S. Kevin, G. Michael and T. Elijah, *Nature*, 2011, **10**, 456–461.

10 R. Marschall, *Adv. Funct. Mater.*, 2014, **24**, 2421–2440.

11 Y. Qu and X. Duan, *Chem. Soc. Rev.*, 2013, **42**, 2568–2580.

12 C. D. Valentin, G. Pacchioni and A. Selloni, *J. Phys. Chem. C*, 2009, **133**, 20543–20552.

13 M. Zou, L. Feng, A. S. Ganeshraja, F. Xiong and M. Yang, *Solid State Sci.*, 2016, **60**, 1–10.

14 Z. Lian, W. Wang, S. Xiao, X. Li, Y. Cui, D. Zhang, G. Li and H. Li, *Sci. Rep.*, 2015, **5**, 10461–10470.

15 K. Nakashima, M. Kera, I. Fujii and S. Wada, *Ceram. Int.*, 2013, **39**, 3231–3234.

16 K. Domem, A. Kudo and T. Onishi, *J. Phys. Chem.*, 1986, **90**, 292–295.

17 M. Cantarella, A. D. Mauro, A. Gulino, L. Spitaleri, G. Nicotra, V. Privitera and G. Impellizzeri, *Appl. Catal., B*, 2018, **238**, 509–517.

18 G. Wang, Z. Li, M. Li, Y. Feng, W. Li, S. Lv and J. Liao, *Ceram. Int.*, 2018, **44**, 1291–1295.

19 S. Tokunaga, H. Kato and A. Kudo, *Chem. Mater.*, 2001, **13**, 4624–4628.

20 F. F. Abdi and R. V. D. Krol, *J. Phys. Chem. C*, 2012, **116**, 9398–9404.

21 W. J. Jo, J. W. Jang, K. J. Kong, H. J. Kang, J. Y. Kim, H. Jun, K. P. S. Parmar and J. S. Lee, *Angew. Chem., Int. Ed.*, 2012, **51**, 3147–3151.

22 H. Ma, K. Teng, Y. Fu, Y. Song, Y. Wang and X. Dong, *Energy Environ. Sci.*, 2011, **4**, 3067–3074.

23 J. S. Jang, S. H. Choi, H. G. Kim and J. S. Lee, *J. Phys. Chem. C*, 2008, **112**, 17200–17205.

24 X. Jiang, L. Wang, F. Yu, Y. Nie, Q. Xing, X. Liu, Y. Pei, J. Zou and We. Dai, *ACS Sustainable Chem. Eng.*, 2018, **6**, 12695–12705.

25 S. Song, C. Lu, X. Wu, S. Jiang, C. Sun and Z. Le, *Appl. Catal., B*, 2018, **227**, 145–152.

26 J. Cao, B. D. Luo, H. L. Lin and S. F. Chen, *J. Hazard. Mater.*, 2011, **190**, 700–706.

27 F. Teng, M. Chen, N. Li, X. Hua, J. Wang, Q. Zhang, Y. Wang, D. D. Meng and G. Li, *RSC Adv.*, 2013, **3**, 743–751.

28 Y. Luo, J. Luo, J. Zhou, X. Qi, H. Zhang, D. Y. W. Yu, C. Li, H. Fan and T. Yu, *J. Mater. Chem. A*, 2013, **1**, 273–281.

29 W. Liu, X. Li, M. Zhu and X. He, *J. Power Sources*, 2015, **282**, 179–186.

30 X. Zheng, Z. Han, W. Yang, F. Qu, B. Liu and X. Wu, *Dalton Trans.*, 2016, **45**, 16850–16858.

31 J. Wang, X. Zhang, Q. Wei, H. Lv, Y. Tian, Z. Tong, X. Liu, J. Hao, H. Qu, J. Zhao, Y. Li and L. Mai, *Nano Energy*, 2016, **19**, 222–233.

32 X. Zhang, P. Guo, Q. Pan, K. Shi and G. Zhang, *J. Alloys Compd.*, 2017, **727**, 514–521.

33 H. Xu, M. Shi, C. Liang, S. Wang, C. Xia, C. Xue, Z. Hai and S. Zhuiykov, *Nanoscale Res. Lett.*, 2018, **13**, 195–210.

34 Q. Xiao, J. Zhang, C. Xiao and X. Tan, *Catal. Commun.*, 2008, **9**, 1247–1253.

35 W. Ahmad, T. Noor and M. Zeeshan, *Catal. Commun.*, 2017, **89**, 19–24.

36 S. H. Hsieh, G. J. Lee, C. Y. Chen, J. Chen, S. H. Ma, T. L. Horng, K. Chen and J. J. Wu, *Top. Catal.*, 2013, **56**, 623–629.

37 X. Liu, J. Iocozzia, Y. Wang, X. Cui, Y. Chen, S. Zhao, Z. Li and Z. Lin, *Energy Environ. Sci.*, 2017, **10**, 402–434.

38 Q. Lu, Z. Lu, Y. Lu, L. Lv, Y. Ning, H. Yu, Y. Hou and Y. Yin, *Nano Lett.*, 2013, **13**, 5698–5702.

39 M. R. Khan, T. W. Chuan, A. Yousuf, M. N. K. Chowdhurya and C. K. Cheng, *Catal. Sci. Technol.*, 2015, **5**, 2522–2531.

40 P. Mazierski, A. Malankowska, M. Kobylanski, M. Diak, M. Kozak, M. J. Winiarski, T. Klimczuk, W. Lisowski, G. Nowaczyk and A. Z. Medynska, *ACS Catal.*, 2017, **7**, 2753–2764.

41 Y. Cao, Z. Xing, Z. Li, X. Wu, M. Hu, X. Yan, Q. Zhu, S. Yang and W. Zhou, *J. Hazard. Mater.*, 2018, **343**, 181–190.

42 T. Sakata, T. Kawai and K. Hashimoto, *J. Phys. Chem.*, 1984, **88**, 2344–2350.

43 X. Wan, R. Ma, S. L. Tie and S. Lan, *Mater. Sci. Semicond. Process.*, 2014, **27**, 748–757.

44 L. Jian, D. Cai, G. Su, D. Lin, M. Lin, J. Li, J. Liu, X. Wan, S. Tie and S. Lan, *Appl. Catal., A*, 2016, **512**, 74–84.

45 Y. Li and Y. Wu, *Chem. Mater.*, 2010, **22**, 5537–5542.

46 S. K. Jesudoss, J. J. Vijaya, P. I. Rajan, K. Kaviyarasu, M. Sivachidambaram, L. J. Kennedy, H. A. Al-Lohedan, R. Jothiramalingam and M. A. Munusamy, *Photochem. Photobiol. Sci.*, 2017, **16**, 766–778.

47 H. Chen, J. Tan, J. Cui, X. Yang, H. Zheng, Y. Zhu and Y. Li, *Mol. Catal.*, 2017, **433**, 346–353.

48 H. Sun, X. Sun, T. Hu, M. Yu, F. Lu and J. Lian, *J. Phys. Chem. C*, 2014, **118**, 2263–2272.

49 Q. Liao, N. Li, S. Jin, G. Yang and C. Wang, *J. Am. Chem. Soc.*, 2015, **9**, 5310–5317.

50 Z. Shang, M. Sun, S. Chang, X. Che, X. Cao, L. Wang, Y. Guo, W. Zhan, Y. Guo and G. Lu, *Appl. Catal., B*, 2017, **209**, 33–44.

51 M. Pudukudy and Z. Yaakob, *Chem. Pap.*, 2014, **68**, 1087–1096.

52 S. Vijayakumar, A. Kiruthika Ponnalagi, S. Nagamuthu and G. Muralidharan, *Electrochim. Acta*, 2013, **106**, 500–505.

53 T. He, D. Chen, X. Jiao, Y. Wang and Y. Duan, *Chem. Mater.*, 2005, **17**, 4023–4030.

54 D. Barreca, C. Massignan, S. Daolio, M. Fabrizio, C. Piccirillo, L. Armelao and E. Tondello, *Chem. Mater.*, 2001, **13**, 588–593.

55 A. Gulino, P. Dapporto, P. Rossi and I. Fragala, *Chem. Mater.*, 2003, **15**, 3748–3752.

56 M. Zhou, J. Yu, S. Liu, P. Zhai and L. Jiang, *J. Hazard. Mater.*, 2008, **154**, 1141–1148.

57 T. T. Y. Tan, C. K. Yip, D. Beydoun and R. Amal, *Chem. Eng. J.*, 2003, **95**, 179–186.

58 L. Chen, Y. Cui, S. Shi, H. Luo and Y. Gao, *Appl. Surf. Sci.*, 2018, **450**, 318–327.

59 M. Liu, J. Liu, Z. Li and F. Wang, *ACS Appl. Mater. Interfaces*, 2018, **10**, 7052–7060.

60 X. P. Qiu, J. S. Yu, H. M. Xu, W. X. Chen, W. Hu, H. Y. Bai and G. L. Chen, *Appl. Surf. Sci.*, 2016, **362**, 498–505.

61 X. P. Qiu, J. S. Yu, H. M. Xu, W. X. Chen, W. Hu and G. L. Chen, *Appl. Surf. Sci.*, 2016, **382**, 249–259.